

# Identifying mutant-specific multi-drug combinations using Comparative Network Reconstruction

Evert Bosdriesz<sup>1,2,\*</sup>, João M. Fernandes Neto<sup>2</sup>, Anja Sieber<sup>3,4</sup>, René Bernards<sup>2</sup>, Nils Blüthgen<sup>3,4,5</sup>, and Lodewyk F.A. Wessels<sup>1,6,\*</sup>

<sup>1</sup> Computer Science Department, Center for Integrative Bioinformatics (IBIVU), VU Amsterdam, The Netherlands

<sup>2</sup> Division of Molecular Carcinogenesis, The Oncode Institute, The Netherlands Cancer Institute, Amsterdam, the Netherlands

<sup>3</sup> Institute of Pathology, Charité Universitätsmedizin, Berlin, Germany

<sup>4</sup> IRI Life Sciences, Humboldt University of Berlin, Berlin, Germany

<sup>5</sup> Berlin Institute of Health, Berlin, Germany

<sup>6</sup> Faculty of EEMCS, Delft University of Technology, Delft, the Netherlands

\*Corresponding authors: e.bosdriesz@vu.nl, l.wessels@nki.nl

## Abstract

Inhibition of aberrant signaling with target inhibitors is an important treatment strategy in cancer, but unfortunately responses are often short-lived. Multi-drug combinations have the potential to mitigate this, but to avoid toxicity such combinations must be selective and the dosage of the individual drugs should be as low as possible. Since the search space of multi-drug combinations is enormous, an efficient approach to identify the most promising drug combinations and dosages is needed.

Here, we present a pipeline to prioritize promising multi-drug combinations. We performed a limited set of drug perturbations in an isogenic cell line pair with and without an activating PI3K mutation, and recorded their signaling states and cell viability. We used these data to reconstruct mutant specific signaling networks and map the short term signaling response to longer term changes in cell viability. The resulting models then allowed us to predict the effect of unseen multi-drug combinations, at arbitrary drug-concentrations, on cell viability. Our initial aim was to find combinations that selectively reduce the viability of the PI3K mutant cells, but our models indicated that such combinations do not exist for this cell line pair. However, we were able to validate 25 of the 30 low-dose multi-drug combinations that we predicted to be anti-selective. Our pipeline thus enables a powerful strategy to rapidly map the efficacy and possible selectivity of drug combinations, hence significantly speeding up the pace at which we can explore the vast space of combination therapies.

## 31 Introduction

32 The dependency of tumors on activated signaling pathways results in therapeutic responses to inhibitors  
33 that block pathway activity [1]. However, resistance to such targeted inhibitors inevitably develops [2, 3].  
34 Combinations of two targeted inhibitors can give more lasting clinical benefit, but resistance nonetheless  
35 emerges [4, 5]. Combining more than two drugs might further extend the duration of the response [6],  
36 but toxicity becomes a major concern when multiple drugs are combined at their maximum tolerated  
37 dose. Recently, we found that partial inhibition of three or four kinases by combining Multiple drugs at  
38 Low Dose (MLD) is surprisingly effective in receptor tyrosine kinase (RTK) driven tumors in multiple  
39 cancer types [7]. It prevents the development of resistance, and it is well tolerated by mice. Others have  
40 also shown the potential of multi-drug (low dose) combinations in pre-clinical [8–11] and clinical [12, 13]  
41 settings.

42 These findings warrant further exploration of multiple-drug combination strategies. This will require a  
43 systematic way to explore promising drug combination treatments, including optimizing the dosing of  
44 the different drugs. The combinatorial explosion of the search space — there are more than 2 million  
45 possible 4-way combinations of the 89 (as of 2020 [14]) FDA approved targeted inhibitors, and 24 billion  
46 if each drug is to be tested at 10 different concentrations — means that in-vitro testing of all combinations  
47 is infeasible. Computational approaches are required to prioritize promising combinations.

48 Recently, Nowak-Sliwinska and collaborators presented a “Feedback Systems Control” approach  
49 to explore the search-space of possible multi-drug combinations [10, 15, 16]. While this approach is  
50 promising, the method does not optimize for selectivity and the obtained results lack a mechanistic  
51 underpinning, making it hard to assess to what extent the results will generalize. Another promising  
52 approach is building mathematical models of cellular signaling, based on a limited set of perturbation  
53 experiments [17–24]. However, current approaches suffer from two major shortcomings. First, only a  
54 very limited number of such modeling approaches focus on the difference between cells with different  
55 mutation profiles [17, 25], which is critical for optimizing selectivity. Second, how inhibition of oncogenic  
56 signaling affects cell viability, and specifically to what extend short-term signaling response is informative  
57 for longer-term cell fate, remains underexplored [23, 24, 26].

58 We therefore set out to establish and validate a combined experimental and computational pipeline  
59 to prioritize multi-drug combinations and their dosing based on mathematical models of drug response  
60 (Figure 1). Importantly, we aimed to find combinations that are selective for cells with a particular  
61 oncogenic driver mutation. To isolate the effect of the mutation, we used an isogenic cell line pair with and  
62 without a mutation. Specifically, we used MCF10A, a cell line derived from epithelial breast tissue [27], and  
63 an isogenic clone with the activating PI3K<sup>H1047R</sup>-mutation knocked in under its endogenous promoter [28].  
64 We measured the response of the MAPK and AKT pathway and cell viability after drug perturbations,  
65 and used the measurements to build mutant specific signaling networks models using Comparative  
66 Network Reconstruction, a method we recently developed [17]. In addition, we found that non-linear  
67 model combining the response of phospho-ERK and phospho-AKT is highly predictive for cell viability,  
68 despite the fact that signaling response and cell viability are measured on completely different time-scales

69 of hours and days, respectively. Combining the model of mutant signaling with the cell viability model  
70 allowed us to simulate the effect of any multi-drug combination at any concentration and thus to prioritize  
71 promising combinations. Our models indicated that no drug combination would likely be selective for  
72 the PI3K-mutant cells. To nonetheless validate our computational approach, we proceeded to predict  
73 which low-dose, multi-drug combinations were likely to be anti-selective, i.e. reduce the viability of the  
74 parental cells more strongly than that of the PI3K-mutants. Experimental validation showed that 25 of the  
75 30 combinations that we predicted to be anti-selective indeed had a significantly stronger effect in the  
76 parental cell than in the PI3K-mutant cells.

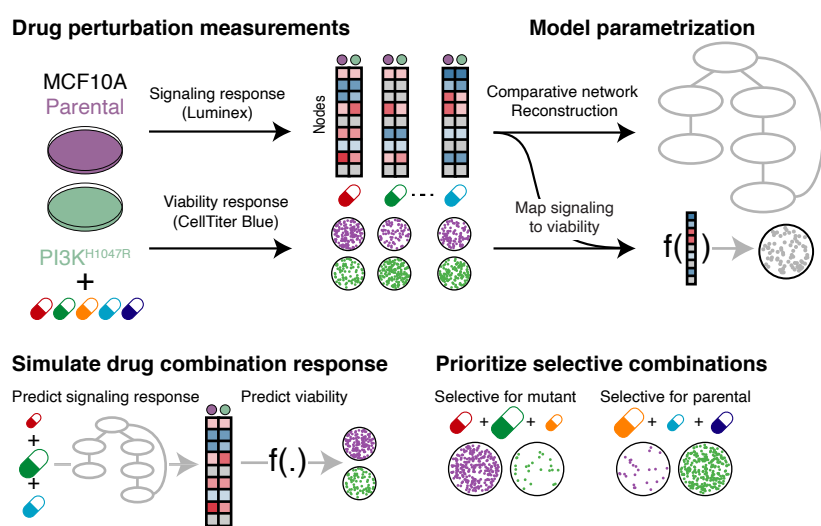


**Figure 1: Overview of pipeline to prioritize promising selective low-dose multi-drug combinations.** **Top:** MCF10A parental and PI3K<sup>H1047R</sup> cells are treated with inhibitors targeting the MAPK and AKT pathways. The signaling and cell viability responses are measured and used to build mutant specific models of signal-transduction networks and to parametrize the relationship between signaling response and cell viability. **Bottom:** These models are used to simulate the response to unobserved multi-drug combinations, at arbitrary concentrations, of the signaling networks and how this affects cell viability. In this way, low-dose multi-drug combinations that are likely selective for a particular cell type can be prioritized.

## 77 Results

### 78 The signaling and viability response to drug perturbations in MCA10A parental 79 and PI3K<sup>H1047R</sup> mutated cells

80 To test how oncogenic mutations affect signal transduction networks and their downstream effects on  
81 cellular phenotypes such as cell viability, we used the MCF10A cell line [27] and an isogenic clone with  
82 the activating PI3K<sup>H1047R</sup> mutation knocked in under its endogenous promoter [28]. As expected, in  
83 the PI3K<sup>H1047R</sup> cells the baseline signaling activity of AKT and PRAS40, both downstream of PI3K, is  
84 elevated, but the other signaling nodes do not show significant differences in activity (Figure 2A). In the  
85 absence of drug perturbations, PI3K<sup>H1047R</sup>-mutant MCF10A cells have a comparable growth rate as their  
86 parental cells [28]. Dose response curves of selected PI3K and the MAPK pathway inhibitors showed  
87 subtle differences in sensitivities between the parental and the mutant cells (Figure S1A).

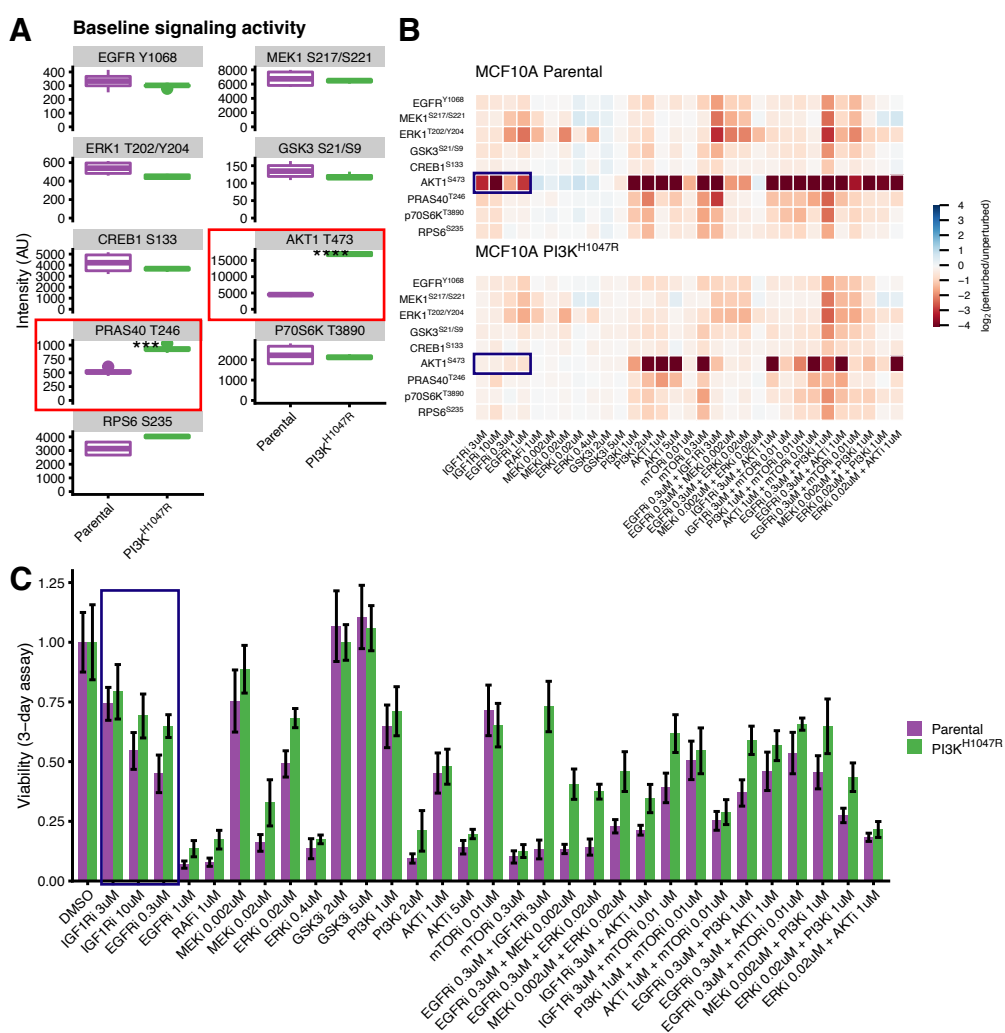


**Figure 2: Profiling signaling and viability response of MCF10A parental en PI3K<sup>H1047R</sup> cells to drug perturbations.** **A.** Node activity in the unperturbed cells. Most nodes have similar activity in the parental and PI3K<sup>H1047R</sup> cells, except AKT and PRAS40 (highlighted) which are downstream of PI3K. **B.** Heatmap representing log<sub>2</sub>-fold changes of the signaling nodes upon drug perturbation compared to DMSO controls. The response of the parental and PI3K<sup>H1047R</sup> cells are highly correlated, with some exceptions such that of AKT1 upon growth-factor receptor inhibition (highlighted). Signaling response is measured after 2 hours of drug treatment. The color scale is capped between -4 and 4 for visualization purposes. **C.** Cell viability under the same drug treatments as reported in panel B. Both cell lines show a similar response profile. The strong differences in AKT response to growth-factor receptor inhibition translate into mild differences in cell viability (highlighted). Cell viability is measured after 3 days of drug treatment. Error-bars represent standard deviations.

88 To study how the signaling of these cells respond to drug-perturbations and if the PI3K<sup>H1047R</sup> mutation  
 89 influences this, we perturbed both cell lines with inhibitors of the PI3K and MAPK pathways, and selected  
 90 2-drug combinations of these. Single drugs were tested at two different concentrations, corresponding  
 91 roughly to their IC<sub>50</sub> and IC<sub>90</sub> values (except RAFi, which was only tested at IC<sub>90</sub>) and drug-combinations  
 92 were tested with both drugs at their IC<sub>50</sub> values, to obtain a total of 34 different perturbations. We  
 93 measured the response after two hours of drug treatment (log<sub>2</sub> fold change relative to DMSO control) of  
 94 nine main nodes in the PI3K and MAPK signaling pathway using a multiplexed luminex assay to obtain  
 95 more than 600 signaling drug-response measurements (Figure 2B, Table S1 and S2). We selected the  
 96 two hour time-point because this is the timescale for phospho-AKT (pAKT) to reach quasi steady state

97 after PI3K-pathway inhibition [29] (Figure S1B). Luminex quantification showed excellent concordance  
98 with Western Blots (Figure S1C). In addition we measured the effect on cell viability using CellTiter  
99 Blue (Figure 2C, Table S3 and S4). Generally, the differences in both signaling response and cell  
100 viability between the parental and PI3K-mutant cells were subtle but consistent. For instance, while the  
101 responses of the signaling nodes of the parental and PI3K<sup>H1047R</sup> cells are strongly correlated (Figure 2B  
102 and Figure S1D), pAKT shows a strong negative response to growth-factor receptor inhibition (EGFRi  
103 or IGF1Ri) that is nearly absent in the PI3K<sup>H1047R</sup> mutant cells (Figure 2B, highlighted). However, this  
104 results in only mild differences in cell viability between the cell lines (Figure 2C, highlighted).

105 **Network reconstructions identify relevant differences between parental and**  
106 **PI3K-mutant cells**

107 To establish how the PI3K<sup>H1047R</sup> mutation affects the signal transduction network, we used the drug-  
108 response measurements to perform Comparative Network Reconstruction (CNR) [17] of the MAPK and  
109 AKT pathways of both cell lines. CNR is a method that we have recently developed to reconstruct and  
110 quantify signaling networks and identify the most important quantitative differences between two or more  
111 cell lines. Prior knowledge about the network topology can be included, but the algorithm can also  
112 propose edges to be added to the network. The edge-weights are interpreted as the percent change in  
113 the downstream node activity in response to a 1% change in activity of the upstream node. Importantly,  
114 by penalizing differences between cell line models, CNR identifies which edges are quantitatively different  
115 between the two cell lines.

116 We used the canonical MAPK and PI3K pathway interactions as prior information, and added 4  
117 edges that were proposed by the CNR algorithm based on hyperparameter selected in a leave-one-out  
118 cross validation loop (Figs 3A and S2A). The targets of some inhibitors were not measured in our panel.  
119 These were modelled as affecting the first downstream target that was measured. For instance, since  
120 both IGF1R and PI3K are not measured in our panel, IGF1R inhibition was modelled as targeting AKT1  
121 directly. The model gave a good fit to the data (Pearson correlation = 0.91) (Figure 3B). To assess the  
122 significance of this fit, we compared the residuals of the model to 1000 models with the same number of  
123 randomly selected edges. Each of these 1000 random models had a worse fit than our model ( $p < 0.001$ ,  
124 Figure 3C).

125 CNR aims to identify the most relevant differences between cell lines by penalizing quantitative  
126 differences. These differences can be either the edges in the network, or the strength of inhibition of  
127 a drug to its direct target. This way, we identified 13 relevant differences between the parental and  
128 PI3K<sup>H1047R</sup> cells. These differences are highlighted in blue in Figure 3A. The numbers next to the edges  
129 indicate the edge-strengths of the parental (purple) and PI3K<sup>H1047R</sup> (green) cells. (For visualization  
130 purposes, only the strength of edges that differ between the cell lines are indicated. For full model  
131 visualization, see Figure S2B). The differences in target-inhibition strength between the cell lines are  
132 shown in Figure 3D-G and Figure S2D. We assessed the significance of the identified differences by  
133 comparing the residuals of our model to that of 1000 models with the same number of randomly selected

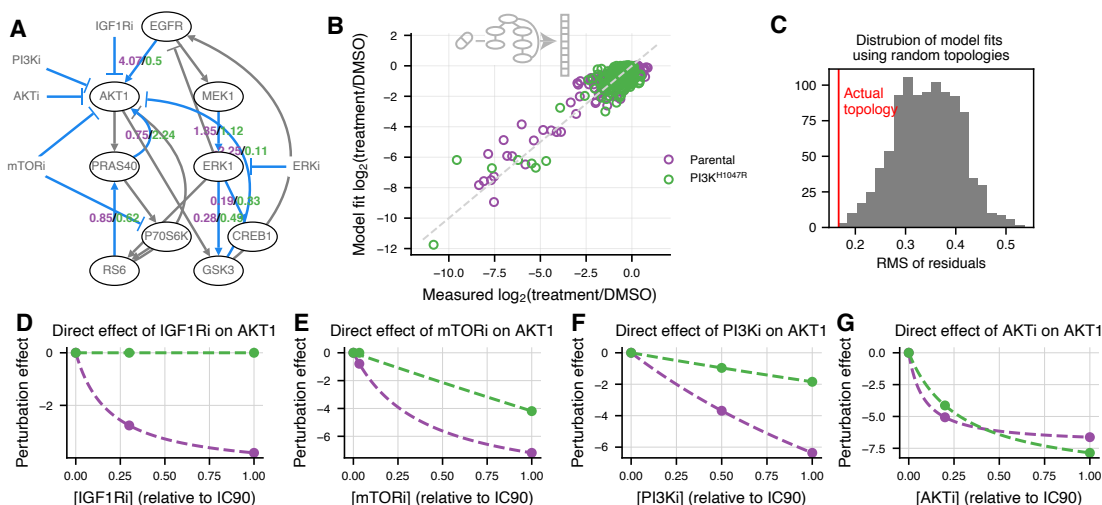


**Figure 3: Mutant specific network reconstructions show expected differences.** **A.** Comparative Network Reconstruction (CNR) of MCF10A parental and PI3K<sup>H1047R</sup> cells. Edges and direct perturbation effects that differ between the two cell lines are highlighted in blue. Gray edges do not differ between the cell lines. Edge strengths of the differing edges are represented by the purple (parental) and green (PI3K<sup>H1047R</sup>) numbers. Ovals indicate nodes. For visualization purposes, only direct perturbation effects that differ between the cell lines are indicated. As expected, the most and the strongest differences between the cell lines are located close to AKT in the network (note that PI3K is not measured). **B.** Comparison of network model fit with measured signaling response shows that the network model can explain the signaling response data well (Pearson correlation 0.91). **C.** Distribution of the root mean square of residuals of models optimized using a random topology (gray), compared to that of the actual model used (red). All 1000 random topology models had the same number of edges as the actual model, and for all 1000 the fit was worse than for the actual model. **D-G.** The estimated direct effect of IGF1R (C), mTOR (D), PI3K (E) and AKT (F) inhibition on AKT activity as a function of applied inhibitor concentration. Points indicate the estimated effects of the concentrations used in the CNR reconstruction, the dashed lines indicate the interpolated curves between these points (c.f. Materials and Methods, Equation 5). IGF1R, PI3K, and mTOR inhibition were modelled as directly affecting AKT because their actual targets were not measured.

134 differences. None of the random models had a better fit to the data (Figure S2C), indicating that the  
 135 identified differences are, indeed, the most relevant differences.

136 As expected, most of the identified differences are located close to AKT in the network (Figure 3A,  
 137 note that PI3K is not measured). Specifically, in the PI3K<sup>H1047R</sup> cells, AKT is less sensitive to changes  
 138 in EGFR and unresponsive to IGF1R inhibition (Figure 3A and D), which is consistent with PI3K being  
 139 constitutively activated. Additionally, AKT is less responsive to PI3K and mTOR inhibition (Figure 3E,F).  
 140 At the IC<sub>50</sub>, AKT is also less sensitive to AKT inhibition, but when AKTi is applied at its IC<sub>90</sub>, the  
 141 PI3K<sup>H1047R</sup> cells show a larger response (Figure 3G). This last observation might be explained by the  
 142 higher baseline AKT activity of PI3K<sup>H1047R</sup> cells, since if AKT activity is reduced to a similar absolute  
 143 level, the fold-change of AKT in the mutant is higher.

144 In order to predict the signaling-response to drugs combined at arbitrary concentrations, we param-  
 145 eterized the relation between target inhibition and drug concentration using the direct target-inhibition  
 146 estimates for drug *k* on node *i* for the IC<sub>50</sub> and IC<sub>90</sub> we obtained from the network reconstructions (c.f.  
 147 Materials and Methods, Equation 5). The dashed lines in Figs 3D-G and Figure S2C indicate the curves  
 148 we parametrized in this way.

149 **Short-term signaling response is informative for long-term cell viability**

150 To prioritize multi-drug combinations, the short term response of the signaling network to a drug  
 151 perturbation needs to be related to its longer term effect on cell viability. Important open questions here  
 152 are: Is the short-term signaling response predictive to longer term cell viability? If so, which signaling  
 153 outputs are most predictive, and what is their relation? The association between the individual node-  
 154 responses and cell viability were moderate even for the most strongly associated nodes, phospho-AKT  
 155 (pAKT) and phospho-ERK (pERK), which had a Pearson correlation with cell viability of 0.36 and 0.42,  
 156 respectively (Figure 4A). The responses of all other nodes also correlated somewhat with cell viability  
 157 (Figure S3A), but clearly no single node alone is a good predictor for cell viability.

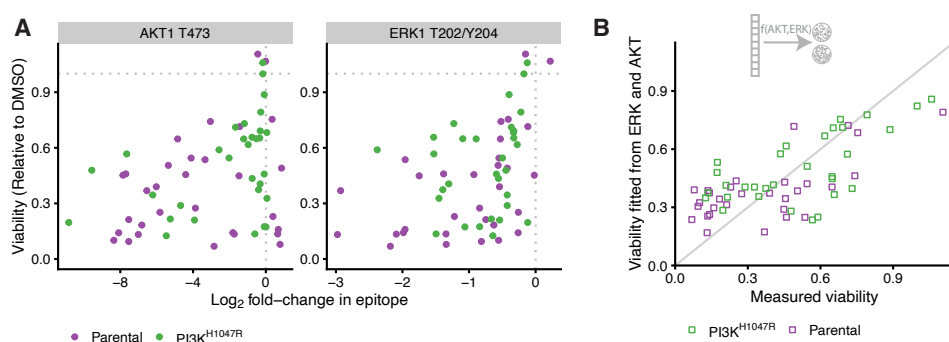


**Figure 4: Short term signaling response is predictive for longer term cell viability.** **A.** Scatterplot of cell viability against log<sub>2</sub>-fold changes in AKT (left panel) and ERK (right panel) activity in response to drug treatments. The Pearson correlations are 0.36 and 0.42 respectively. **B.** Scatterplot of model fit against measured cell viability based on a model where both ERK and AKT response are used to explain cell viability (c.f. Materials and Methods, Equation 4). The Pearson correlation between fit and measurement is 0.71.

158 We therefore investigated whether a model combining the response of multiple nodes described  
 159 the cell viability data better. To this end, we first fitted a linear model using either all nodes or only the  
 160 response of pERK and pAKT. Both models gave a reasonable fit to the data, but there was a clear  
 161 structure in the relation between the residuals and the fitted values (Figure S4A and B), indicating that  
 162 a non-linear model might be more suitable. To test this, we fitted a number of biologically motivated  
 163 non-linear models relating the combined response of pAKT and pERK to cell viability. These non-linear  
 164 models that all have the property that cell viability goes to 0 if either pERK or pAKT are fully inhibited (c.f.  
 165 Materials and Methods, Equation 4). The biological assumption behind this is that both ERK and AKT  
 166 activation are required for cell survival and growth.

167 To select the best model, we compared the standardized residuals of the model fits and the L2-  
 168 norm of the residuals in a leave one-out cross-validation loop of the different models (Table 1). All  
 169 non-linear models had clearly better performance than the linear models, despite having equal or less  
 170 free parameters. While overall the predictions of the different non-linear models were fairly similar (with  
 171 Pearson correlations of their predictions between 0.92 and 0.99, Figure S4D), a Michaelis-Menten like  
 172 model of the following form

$$v_k = \frac{1}{1 - \frac{R_{AKT,k}}{K_{M,AKT}} - \frac{R_{ERK,k}}{K_{M,ERK}}} \quad (1)$$

173 had the overall best performance on both metrics and shows no clear structure in the residuals (Fig-

ure S4C). Here,  $v_k$  is the cell viability and  $R_{ERK,k}$  and  $R_{AKT,k}$  are the log<sub>2</sub>-fold changes of pERK and pAKT upon drug treatment  $k$ . The parameters  $K_{M,ERK}$  and  $K_{M,AKT}$  can be interpreted as the log<sub>2</sub>-fold changes of pERK and pAKT that cause 50% inhibition of cell viability. They differ slightly between the two cell lines, but the bootstrapped 95% confidence intervals strongly overlap (Figure S4E), so we do not want to overinterpret these differences. Importantly, this model gave a good fit to the data (Figure 4B), with a Pearson correlation between fitted and measured viability of 0.71.

Function	Type	$\sigma$ (Model fit)	$L_2$ -norm (LOOCV)
$v_k \sim 1 / \left( 1 - \frac{R_{AKT,k}}{K_{M,AKT}} - \frac{R_{ERK,k}}{K_{M,ERK}} \right)$	Non-linear	0.20	0.042
$v_k \sim 1 / \left[ \left( 1 - \frac{R_{AKT,k}}{K_{M,AKT}} \right) \cdot \left( 1 - \frac{R_{ERK,k}}{K_{M,ERK}} \right) \right]$	Non-linear	0.20	0.045
$v_k \sim 3 / \left( 1 + 2^{-\frac{R_{ERK,k}}{K_{M,ERK}}} + 2^{-\frac{R_{AKT,k}}{K_{M,AKT}}} \right)$	Non-linear	0.21	0.048
$v_k \sim 4 / \left[ \left( 1 + 2^{-\frac{R_{ERK,k}}{K_{M,ERK}}} \right) \cdot \left( 1 + 2^{-\frac{R_{AKT,k}}{K_{M,AKT}}} \right) \right]$	Non-linear	0.21	0.048
$1 - v_k \sim \sum_{i \in \text{nodes}} \beta_i R_{ik}$	Linear	0.21	0.061
$1 - v_k \sim \beta_{AKT} \cdot R_{AKT,k} + \beta_{ERK} R_{ERK,k}$	Linear	0.28	0.093

**Table 1: Comparison of goodness of fit of functions relating signaling response to cell viability.**  $\sigma$  is the mean residual standard error of the model fitted to the full data. The  $L_2$ -norm is calculated over predictions made in a leave-one-out cross-validation loop. The non-linear models predict viability  $v$  from the log<sub>2</sub>-fold change of pERK and pAKT ( $R_{ERK}$  and  $R_{AKT}$ ) whereas the linear models fit the inhibition ( $1 - v$ ). The table is ordered from best to worst fit.

Together, these results indicate that short-term signaling response is informative for longer-term drug response, that pAKT and pERK are the most informative readouts, and that the relation between signaling response and viability is non-linear.

### Prediction and validation of selective multi-drug-combinations

We then combined the network models (Figure 3A) with the parametrization of the signaling-viability model (Equation 4) to simulate the effect on cell viability of unseen 3-drug combination at unseen drug-concentrations. When applying this model to the training data, the Pearson correlation between measured and fitted cell viability was 0.78 (Figure 5A). We used this model to prioritize multi-drug combinations and their dosing that maximize the selectivity, defined as the difference in viability between the parental and the PI3K<sup>H1047R</sup> cells.

To do this, for all possible 3-drug combinations we optimized the concentrations such that the viability of the PI3K<sup>H1047R</sup> mutants is minimized, under the constraint that the viability of the parental cells remains above 0.8 relative to DMSO control (c.f. Materials and Methods, Equation 7). To look for low-dose drug combinations, we added the constraint that each drug can be used maximally at its IC<sub>10</sub>. However, no drug-combination was predicted to be selective for the PI3K<sup>H1047R</sup> cells at any combination of concentrations. Since none of the single drugs shows selectivity towards the PI3K<sup>H1047R</sup> cells (Figure 2C), this is not very surprising. Moreover, our network reconstructions indicated that the main effect of the PI3K<sup>H1047R</sup> mutation is to render the MCF10A parental line independent of growth-factor stimulation. Indeed, when we grew MCF10A parental and PI3K<sup>H1047R</sup> cells in the media without

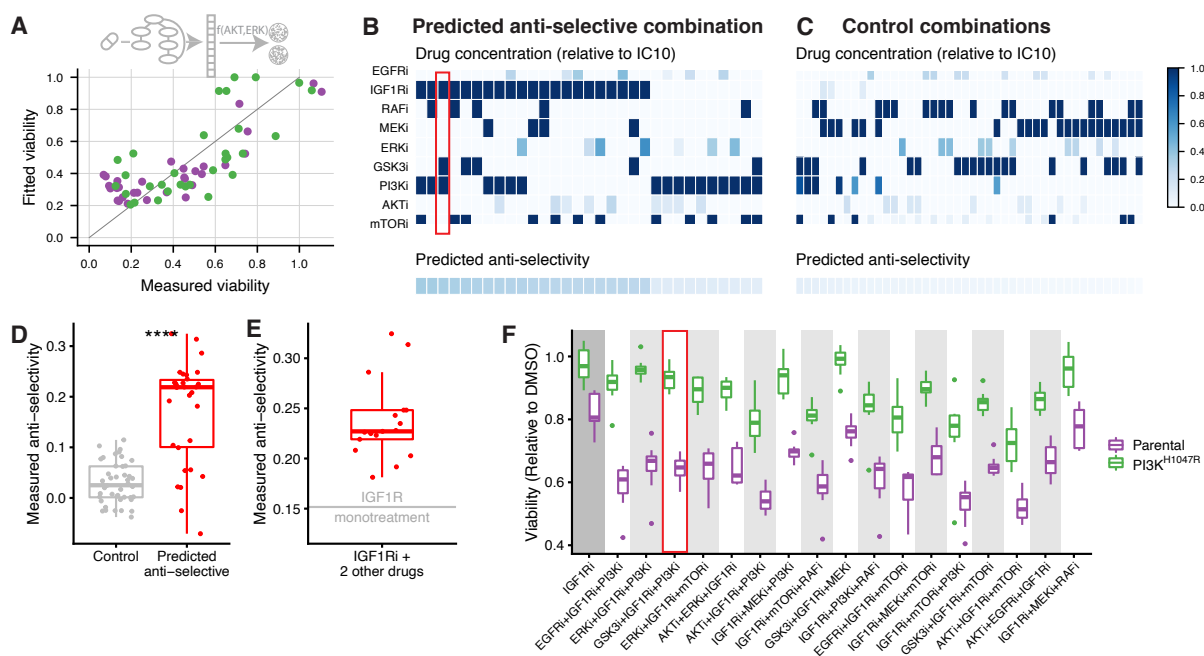


**Figure 5: Experimental validation of anti-selective drug combination predictions.** **A.** Scatterplot comparing full model fit (network model combined with signaling response-viability mapping) to the training data. The Pearson correlation between fit and measurement is 0.78. **B-C.** Overview of drug combinations that we predicted to be anti-selective (B) and non-selective (C) based on this model. Drug concentrations are color-coded relative to their IC<sub>10</sub>. Bottom row indicates predicted anti-selectivity (defined as the difference in viability between PI3K<sup>H1047R</sup> and parental cells) of the combination. These combinations were subsequently tested in the validation experiments. **D.** Box plot comparing the measured anti-selectivity of the drug combinations predicted to anti-selective (panel B) or non-selective (panel C). Each point represents the mean anti-selectivity of one drug combination, which were each tested in 8 replicates. The difference is highly significant (Wilcoxon signed-rank test  $p < 10^{-7}$ ). **E.** Comparison of the measured anti-selectivity of IGF1R mono treatment, indicated by the horizontal gray line, with the selected IGF1R-containing 3-drug combinations (red box plot). IGF1R containing combinations are significantly more anti-selective than IGF1R mono treatment (one-sample t-test  $p < 10^{-7}$ ). **F.** Box plots comparing cell-viability of parental and PI3K<sup>H1047R</sup> cells of the 11 (out of 17) IGF1R containing drug-combinations that are significantly more anti-selective than IGF1R mono treatment.

199 growth-factor, this is what we observed (Figure S5).

200 To nonetheless validate our computational approach, we then looked for drug-combinations that we  
 201 predicted to be anti-selective, i.e. be more effective in the parental cells than in the PI3K-mutants. In our  
 202 optimizations, we found 30 such combinations with an anti-selectivity  $> 0.1$  (Figure 4B). Interestingly,  
 203 IGF1R inhibition was part of all of the 17 combinations that we predict to be most anti-selective, while  
 204 its anti-selectivity in the training data was only modest (Figure 2C). However, the difference in signaling  
 205 response, and specifically pAKT, was much more pronounced (Figure 2B), and this latter aspect gets  
 206 picked up in the network reconstructions (Figure 3A). A particularly interesting example is the combination  
 207 IGF1Ri + PI3Ki + GSK3i. Here, both PI3Ki and GSK3i at their lower dose (IC<sub>50</sub>) show no anti-selectivity,  
 208 yet this combination is predicted to be one of the more anti-selective ones. (Figure 5B, highlighted). As  
 209 a control, we also selected 44 combinations that we predicted to be non-selective for either cell line  
 210 (Figure 5C). A conservative power analysis, based on the accuracy of the viability predictions and the  
 211 effect size of the anti-selectivity predictions, indicated a power of 90% to detect an overall difference in  
 212 selectivity between the anti-selective and control combinations.

213 We then treated the parental and PI3K<sup>H1047R</sup> cells with the 30 predicted to be anti-selective and

214 44 control combinations and measured their viability (Table S5). Combinations that we predicted to be  
215 anti-selective were indeed so, and this was highly significant when compared to the non-selective control  
216 combinations (Wilcoxon signed-rank test  $p < 10^{-7}$ , Figure 5D). Individually, 25 of the 30 combinations  
217 predicted to be anti-selective were indeed significantly so (one-sided t-test  $p < 0.05$ , Table S6).

218 As mentioned above, of the 30 predicted-to-be-anti-selective combinations we tested, 17 contain the  
219 IGF1R inhibitor, which is also mildly anti-selective as monotherapy. (None of the other inhibitors showed  
220 anti-selectivity as a monotherapy at their IC<sub>10</sub>, Figure S6). To rule out the possibility that our result is  
221 mainly driven by the anti-selectivity of IGF1Ri mono-therapy, we compared the 17 IGF1Ri containing  
222 drug combinations with IGF1Ri monotherapy. Figure 5E shows that each of the IGF1Ri containing  
223 combinations we tested (red box plot) is more anti-selective than IGF1Ri treatment alone (indicated by  
224 horizontal gray line). This effect is highly significant (one-sample t-test  $p < 10^{-7}$ ). When looking at the  
225 individual drug combinations, we found that 11 of the 17 IGF1Ri containing combination treatments are  
226 significantly more anti-selective than IGF1Ri monotherapy (one sided t-test  $p < 0.05$ , Figure 5E, Table  
227 S7). This also includes the IGF1Ri + PI3Ki + GSK3i combination highlighted above, which is the second  
228 most anti-selective combination when ranked by effect size.

229 These results indicate that our pipeline is capable of making an accurate prioritization of mutation-  
230 specific low-dose multi-drug combinations. Importantly, these predictions are not always obvious, and  
231 would not have been possible without the help of mathematical models of the signal transduction networks  
232 and their relation to cell viability.

## 233 Discussion

234 In this study, we have shown that it is possible to predict which multiple low dose (MLD) 3-drug combi-  
235 tions are likely to have a mutant specific impact based on a combination of single and 2-drug high dose  
236 drug response measurements and mathematical modeling. We have used drug-perturbation experiments  
237 to reconstruct, quantify and compare signal-transduction networks of an isogenic cell line pair, and linked  
238 the responses of these networks to cell viability. No single signaling readout alone is highly predictive, but  
239 a non-linear model combining the response of ERK and AKT gave a good fit. Importantly, this showed  
240 that the short-term signaling response is predictive for cell viability, which is measured in longer-term  
241 experiments. Based on the so-obtained models we were able to predict and validate drug combinations  
242 that are were specifically effective in one cell line but not another, even though the differences between  
243 the cell lines are subtle.

244 One of our aims was to identify selective drug combinations, i.e. combinations that inhibit cells  
245 with an oncogenic PI3K<sup>H1047R</sup> mutation more strongly then to their parental counterparts. However,  
246 according to our model, no such drug combination exist for this particular model system. The absence  
247 of oncogene-specific sensitivities is presumably due to an absence of “oncogene addiction” [1] to the  
248 PI3K mutation (or any other) in the PI3K<sup>H1047R</sup> MCF10A cells. In the absence of drug-treatment the  
249 mutation has no effect on proliferation under the growth conditions we used, and this mutation therefore  
250 presumably does not induce any vulnerabilities in this cell line. Our network reconstruction suggests that

251 the main effect of the PI3K<sup>H1047R</sup> mutation on MCF10A cells is to make them growth-factor independent,  
252 consistent with previous observations [30]. Hence, the inability to identify selective drug combinations is  
253 due to the particularities of the MCF10A isogenic cell line pair model, and not due to the computational  
254 model.

255 While isogenic cell line pairs with a mutation knocked in are attractive models because they allow  
256 study of the effect of the mutation in isolation, they may thus not always be the best model to study  
257 oncogene-specific sensitivities. An interesting alternative approach might be to use cancer cell lines  
258 of which one of the driver mutations is removed [31–33]. Alternatively, a larger, more heterogeneous  
259 panel of cell lines with and without a particular biomarker could be used [19, 22, 34, 35]. In this scenario,  
260 one would look at commonalities in the signaling network response of the cell lines with the biomarker  
261 compared to the lines without it, and use this to propose combinations that are selective of the biomarker  
262 carrying cell lines. Finally, the use of matched tumor and normal organoids from the same patient could  
263 be used for truly personalized models.

264 Our aim more generally was to develop a combined experimental and computational pipeline to  
265 prioritize drug combinations that have a biomarker specific effect, and in this we did succeed. The majority  
266 of the combinations that we predicted to be anti-selective indeed were so in validation experiments. In  
267 fact, we succeeded in validating our predictions despite the fact that the differences between the cell lines  
268 in the training data were very subtle. It is to be expected that it will be easier to find mutation specific drug  
269 combinations when the effect of a mutation on the signaling networks and on cell viability is stronger.

270 All of the most strongly anti-selective drug combinations we identified contained the IGF1R inhibitor,  
271 but as monotherapy low-dose IGF1Ri is only mildly anti-selective. More generally, which multi-drug  
272 combinations are most selective or anti-selective is often far from obvious. For instance, while in  
273 the training data PI3Ki and GSK3i at their lower dose (IC<sub>50</sub>) individually show no selectivity towards  
274 the parental cells at all, the combination IGF1Ri + PI3Ki + GSK3i is one of the most selective drug  
275 combinations, both as predicted by our model and as measured validation experiments. This underscores  
276 the need for mathematical modelling in prioritizing promising combinations.

277 In conclusion, here we have shown that it is feasible to make accurate, non-trivial predictions about  
278 (anti-)selectivity of multi-drug combinations based on mathematical models of signaling transduction  
279 networks. In combination with suitable model systems, this framework makes it possible to rationally  
280 design biomarker-selective low-dose multidrug combinations.

## 281 Materials and Methods

### 282 Cells and cell culture

283 Human parental and PI3K<sup>H1047R/+</sup> MCF10A cell lines were obtained from Horizon discovery (HD PAR-  
284 003 and HD 101-011). Cells were cultured in DMEM/F-12 including 2.5 mM L-glutamine and 15 mM  
285 HEPES, supplemented with 5% horse serum, 10 µg/mL insulin, 0.5 µg/mL hydrocortisone and 0.1 µg/mL  
286 cholera toxin. Mycoplasma tests were performed every 2 months.

## 287 Reagents and compounds

288 The following inhibitors were used in this study: EGFRi (Gefitinib), IGF1Ri (OSI-906), RAFi (LY3009120),  
289 MEKi (Trametinib), ERKi (SCH772984), GSK3i (3F8), PI3Ki (BKM120), AKTi (MK-2206), mTORi  
290 (AZD8055). All inhibitors were purchased from MedKoo Biosciences. The luminex antibodies against  
291 CREB1<sup>S133</sup>, EGFR<sup>Y1068</sup>, ERK1<sup>T202/Y204</sup>, GSK3<sup>S21/S9</sup>, MEK1<sup>S217/S221</sup>, p70RSK<sup>T389</sup>, PRAS40<sup>T246</sup> and  
292 RPS6<sup>S235</sup> were purchased from ProtATonce Ltd. The luminex antibody against AKT1<sup>T473</sup> was purchased  
293 from BioRad.

## 294 Drug perturbation and validation experiments

295 All the cell-viability measurements were performed in biological triplicates, each with 2 technical replicates,  
296 using black-walled 384-well plates (Greiner 781091). Cells were plated at the optimal seeding density  
297 (200 cells per well) and incubated for approximately 24 hours to allow attachment to the plate. Drugs  
298 were then added to the plates using the Tecan D300e digital dispenser. 10  $\mu$ M phenylarsine oxide  
299 was used as positive control (0% cell viability) and DMSO was used as negative control (100% cell  
300 viability). Three days later, culture medium was removed and CellTiter-Blue (Promega G8081) was added  
301 to the plates. After 2 hours incubation, measurements were performed according to manufacturer's  
302 instructions using the EnVision (PerkinElmer). Viabilities were normalized per cell line according to  
303  $(\text{treatment} - \text{PAO}_{\text{mean}}) / (\text{DMSO}_{\text{mean}} - \text{PAO}_{\text{mean}})$ . IC<sub>50</sub> and IC<sub>90</sub> values were fitted using the R-package  
304 MixedIC50 [36] (code available at <https://github.com/NKI-CCB/MixedIC50>).

305 The signaling response measurements were performed using 6-well plates (Greiner 657165). 300K  
306 cells per well were plated and incubated for approximately 24 hours to allow attachment to the plate.  
307 Drugs were then added to the plates and protein was harvested after 2 hours using the Bio-Plex Pro  
308 Cell Signaling Reagent Kit (BioRad 171304006M) according to the manufacturer's instructions. Protein  
309 concentration of the samples was normalized after performing a Bicinchoninic Acid (BCA) assay (Pierce  
310 BCA, Thermo Scientific), according to the manufacturer's instructions. Cell lysates were analyzed  
311 using the Bio-Plex Protein Array system (Bio-Rad, Hercules, CA) according to the suppliers protocol  
312 as described previously [19]. Intensities were normalized by subtracting blanks for each epitope and  
313 correcting for protein concentration.

## 314 Computational pipeline and data analysis

### 315 Comparative network reconstruction

316 MAPK and AKT signaling networks of the parental and PI3K<sup>H1047R</sup> mutant cell lines were reconstructed  
317 based on the Luminex drug-response data using Comparative Network Reconstruction (CNR)[17]. Briefly,  
318 CNR is a network reconstruction method based on Modular Response Analysis [37]. It links the matrix  
319 of measured node responses to a set of perturbations,  $\mathbf{R}^x$  (where  $R_{ik}^x$  is defined as log<sub>2</sub> fold change  
320 of node  $i$  in response to perturbation  $k$  in cell line  $x$ ) to the matrix unobserved interaction strengths  $\mathbf{r}^x$   
321 (where  $r_{ij}^x$  is the logarithmic partial derivative of node  $i$  with respect to node  $j$  in cell line  $x$ ) and direct

322 perturbation effects  $\mathbf{s}^x$  (with  $s_{ik}^x$  the scaled direct effect of perturbation  $k$  on node  $i$  in cell line  $x$ ). These  
 323 matrices are related through

$$\mathbf{r}^x \cdot \mathbf{R}^x + -\mathbf{s}^x = 0, \quad \forall x. \quad (2)$$

324 In principle,  $\mathbf{r}^x$  and the values of the elements in  $\mathbf{s}^x$  (the targets of the inhibitors is assumed to known)  
 325 can be obtained solving this set of equations, but in practice it is often under-determined. CNR solves  
 326 problem by reformulating it as optimization procedure to find a model that balances data-fit with a model  
 327 complexity by penalizing the number of edges (non-zero entries in  $\mathbf{r}$ ) and differences between cell lines  
 328 (entries in  $\mathbf{r}$  that are quantitatively different between the cell lines). The optimization problem reads:

$$\begin{aligned} \text{Minimize: } & \sum_n \sum_{i,j} \sum_x \epsilon_{in}^x \cdot \epsilon_{in}^x + \eta \cdot I_{ij}^{\text{edge}} + \theta \cdot (I_{ij}^{\text{diff}} + I_{in}^{\text{sdiff}}) \\ \text{Subject to: } & \sum_k r_{ik}^x \cdot R_{kn}^x + s_{in}^x = \epsilon_{in}^x \quad \forall i, j, n, x \\ & I_{ij}^{\text{edge}} = 0 \Rightarrow r_{ij}^x = 0 \quad \forall i, j, x \\ & I_{ij}^{\text{diff}} = 0 \Rightarrow r_{ij}^x - r_{ij}^{\text{mean}} = 0 \quad \forall i, j, x \\ & I_{in}^{\text{sdiff}} = 0 \Rightarrow s_{in}^x - s_{in}^{\text{mean}} = 0 \quad \forall i, n, x \quad (3) \\ & r_{ij}^{\text{mean}} = 1 / N_{\text{cell lines}} \sum_x r_{ij}^x \quad \forall i, j \\ & s_{in}^{\text{mean}} = 1 / N_{\text{cell lines}} \sum_x s_{in}^x \quad \forall i, n \\ & I^{\text{edge}}, I^{\text{diff}}, I^{\text{sdiff}} \in \{0, 1\} \\ & n \in \{\text{perturbations}\}; i, j, k \in \{\text{nodes}\}; x \in \{\text{parental, PI3K}^{\text{H1047R}}\} \end{aligned}$$

329 where the  $\epsilon$ s are the model residuals. Solving this optimization problem gives the matrices  $\mathbf{r}$  and  $\mathbf{s}$  from a  
 330 given  $\mathbf{R}$ .

331 Additional constraints reflecting the experimental design were added to the CNR problem.

- 332 •  $s_{ik}$  is negative and stronger for higher drug concentrations, i.e.  $0 > s_{ik}([IC_{50}]) > s_{ik}([IC_{90}])$ .
- 333 • Each inhibitor-target pair has a single indicator for the difference in perturbations strengths for both  
 334 inhibitor concentrations, i.e. if  $I_{ik}^{\text{sdiff}} = 0 \Rightarrow s_{ik}^{\text{parental}}([IC_{50}]) = s_{ik}^{\text{PI3K}}([IC_{50}])$  and  $s_{ik}^{\text{parental}}([IC_{90}]) =$   
 335  $s_{ik}^{\text{PI3K}}([IC_{90}])$ .
- 336 • Most inhibitors are modelled as a perturbation to their direct target, i.e. EGFRi, MEKi, ERKi, GSK3i  
 337 and AKTi are modelled as perturbations to EGFR, MEK1, ERK1, GSK3 and AKT1 respectively.
- 338 • The MEK inhibitor interferes not only with MEK phosphorylation, but also its catalytic efficiency.  
 339 Hence, MEK inhibition was additionally modelled also modelled as perturbation to it's downstream  
 340 proteins (c.f. [17]).
- 341 • Some inhibitors target kinases that were not measured in our assay. The effect of these inhibitors  
 342 was modelled as a perturbation to the (canonical) downstream nodes of the kinases being inhibited.

343 Specifically, IGF1R inhibition was modelled as a perturbation to MEK1 and AKT1, PI3K inhibition  
344 as a perturbation to AKT1, RAF inhibition as a perturbation to MEK1, and mTOR inhibition as a  
345 perturbation to AKT1 and p70S6K.

346 Prior information about network topology was provided setting the indicators of a set of canonical  
347 MAPK and PI3K pathway interactions  $I_{ij}^{\text{edge}} = 1$ . These indicator constraints are added to the optimization  
348 problem described in Equation 3. The corresponding edge-strengths, together with those of edges that  
349 might be added to the network, are found by solving the optimization problem. Hyperparameter were  
350 set to  $\eta = 0.1$  and  $\theta = 2.0$  based on a leave one out cross validation loop. Single drug treatments were  
351 not included in the leave one out cross validation because each drug concentration needs to be present  
352 in at least one perturbation to estimate the corresponding parameter. The final model was obtained by  
353 restricting the topology to the prior network information with addition of the 4 edges that were identified in  
354 the leave one out cross-validation, and then performing the optimization with  $\theta = 2.0$ .

355 The full Comparative Network Analysis can be found in the Jupyter notebook under the following link:  
356 <https://github.com/evertbosdriesz/cnr-selective-combos/blob/master/python/cnr-mcf10a-pi3k.ipynb>

### 357 **Randomized models**

358 To obtain the distribution of residuals for random network topologies shown in Figure 3C, 1000 models  
359 with a random topology were generated by randomly selecting 16 (out of all possible 72) edges setting  
360 the corresponding indicator to  $I_{ij}^{\text{edge}} = 1$  and setting the indicators of all other edges were set to 0. To  
361 focus on the effect of model topology only, we did not allow for any difference between the cell lines  
362 by setting  $\theta$  to infinity using `cplex.infinity`. Subsequently, edge weights were obtained by solving  
363 the CNR optimization problem described in Equation 3 and corresponding RMS of residuals, defined  
364 as  $\sqrt{\sum_{i,n,x} \epsilon_{in}^x 2 / N}$ , was calculated. To make a fair comparison, we also calculated the residual of our  
365 actual model without any differences between the cell lines. To this end, we set the indicators of the  
366 edges of the actual model  $I_{ij}^{\text{edge}} = 1$  and all others to 0, set  $\theta = \text{cplex.infinity}$ , and re-optimized 3.

367 Similarly, to obtain the distribution of residuals for random differences between the cell lines shown in  
368 Figure S2B, 1000 models with randomly selected  $I^{\text{diff}}$  and  $I^{\text{sdiff}}$  were generated. For all these models,  
369 the topology was first fixed to the topology of the actual model by setting the indicators  $I_{ij}^{\text{edge}} = 1$  for the  
370 edges that are present in the actual model, and all others to 0. Subsequently, 13 randomly selected  
371 indicator for differences between the cell lines  $I^{\text{diff}}$  and  $I^{\text{sdiff}}$  were set to 1, the others to 0, and the  
372 optimization in Equation 7 was solved using these constraints.

373 **The relation between signaling output and cell viability**

The viability (relative to DMSO control) upon perturbation  $k$ ,  $v_k$ , were fitted to the following functions:

$$1 - v_k = \sum_{i \in \text{nodes}} \beta_i R_{ik} \quad (4a)$$

$$1 - v_k = \beta_{AKT} \cdot R_{AKT,k} + \beta_{ERK} R_{ERK,k} \quad (4b)$$

$$v_k = \frac{1}{1 - \frac{R_{AKT,k}}{K_{M,AKT}} - \frac{R_{ERK,k}}{K_{M,ERK}}} \quad (4c)$$

$$v_k = \frac{1}{1 - \frac{R_{AKT,k}}{K_{M,AKT}}} \times \frac{1}{1 - \frac{R_{ERK,k}}{K_{M,ERK}}} \quad (4d)$$

$$v_k = \frac{3}{1 + 2^{-\frac{R_{ERK,k}}{K_{M,ERK}}} + 2^{-\frac{R_{AKT,k}}{K_{M,AKT}}}} \quad (4e)$$

$$v_k = \frac{2}{1 + 2^{-\frac{R_{ERK,k}}{K_{M,ERK}}}} \times \frac{2}{1 + 2^{-\frac{R_{AKT,k}}{K_{M,AKT}}}} \quad (4f)$$

374 Where  $R_{AKT,k}$  and  $R_{ERK,k}$  are the  $\log_2$ -fold changes of pAKT and pERK relative to DMSO control  
 375 upon perturbation  $k$ , respectively.  $K_{M,AKT}$  and  $K_{M,ERK}$  are the parameters to be fitted for the nonlinear  
 376 equations and can be interpreted as the  $R_{AKT,k}$  and  $R_{ERK,k}$  values for which the viability is reduced by  
 377 50% (or 25% and 33% for equations 4e and 4f, respectively). Fitting was performed using the `lm` and `nls`  
 378 functions of R [38] for the linear and non-linear models, respectively. Mean residual standard errors ( $\sigma$ )  
 379 were obtained using the `sigma` function. Leave one out cross-validation was performed on a per cell-line  
 380 basis. Bootstraps were performed using the function `bootstrap` from the 'rsample' package [39].

381 All code and details for this analysis can be found in the RMarkdown-file under the following  
 382 link: <https://github.com/evertbosdriesz/cnr-selective-combos/blob/master/R/02-perturbations/mapping->  
 383 `signaling-drugresponse.Rmd`

384 **Multi-drug response simulations and prediction of selective 3-drug combinations**

385 CNR gives an estimate of the direct target inhibition of each drug only for the concentrations at which the  
 386 drug was applied. To be able to simulate the effect of unseen drug concentrations, the relations between  
 387 the applied concentration of drug  $k$ ,  $[I_k]$ , and target inhibition of node  $i$  in response to this,  $s_{ik}$  were fitted  
 388 to the following function for each inhibitor-target pair,

$$s_{ik}([I_k]) = \frac{I_{max,ik} * [I_k]}{K_{I,ik} + [I_k]}. \quad (5)$$

389 The parameters  $I_{max,ik}$  and  $K_{I,ik}$  were fitted to this function using the  $s_{ik}$ -values for the  $[I_k] = IC_{50}$  and  
 390  $IC_{90}$  obtained from the CNR optimizations with the `curve_fit` function from the python 'scipy.optimize'  
 391 package [40]. For convenience all drug concentrations were normalized to the highest concentration  
 392 applied (the  $IC_{90}$ ), and in all analyses only interpolations and not extrapolations are used ( $0 \leq [I] \leq 1$ ).  
 393  $\mathbf{R}_{A+B+C}$ , the vector of simulated  $\log_2$ -fold changes in response to a perturbation with 3 drugs  $A$ ,  $B$

394 and  $C$ , at concentration  $[I_A]$ ,  $[I_B]$  and  $[I_C]$  was calculated as

$$R_{A+B+C} = r^{-1} (\mathbf{s}_A([I_A]) + \mathbf{s}_B([I_B]) + \mathbf{s}_C([I_C])), \quad (6)$$

395 to obtain  $R_{AKT,A+B+C}$  and  $R_{ERK,A+B+C}$ . These were then used to calculate viability according to  
396 Equation 4. Together, this allows for simulating the effect on cell viability of drug combinations and  
397 concentrations that were not seen in the training data.

For each possible 3-drug combination, the selectivity for cell line  $x$  relative to  $y$  was optimized by solving the following optimization problem:

$$\begin{aligned} \text{Minimize: } & v_{A+B+C}^x \\ \text{Subject to: } & v_{A+B+C}^y \geq v^{y,min} \\ & 0 < [I_k] < IC_{10} \quad k \in \{A, B, C\} \end{aligned} \quad (7)$$

398 where  $v^{y,min}$  is the cutoff used for the minimal viability that cell line  $y$  should have under the 3-drug  
399 treatment, and that we (somewhat arbitrarily) set to 0.8.

Similarly, unselective control combinations were obtained by solving the optimization problem:

$$\begin{aligned} \text{Minimize: } & (v_{A+B+C}^x - 0.8)^2 + (v_{A+B+C}^y - 0.8)^2 \\ \text{Subject to: } & 0 < [I_k] < IC_{10} \quad k \in \{A, B, C\} \end{aligned} \quad (8)$$

400 for all possible 3-drug combinations.

401 A power analysis of the predictions was performed by performing 1000 simulations with addition  
402 gaussian noise with a mean 0 and a standard deviation 0.25 (based on the residuals of our viability  
403 predictions) to the results, and counting in what fraction their was an observable difference between the  
404 two groups.

405 The optimizations were performed in Wolfram Mathematica [41] (version 12.0) using the `NMinimize`  
406 function. The full optimization and power analysis can be found in the Mathematica notebook under the  
407 following link: <https://github.com/evertbosdriesz/cnr-selective-combos/blob/master/mathematica/optimize-combinations.nb>

## 409 **Data and Code availability**

410 All data and code required to reproduce the results and figures in this paper are available at  
411 <https://github.com/evertbosdriesz/cnr-selective-combos>.

## 412 **Acknowledgements**

413 This work was supported by funding from the Oncode Institute and the Gravity Program CGC.nl, funded  
414 by The Netherlands Organisation for Scientific Research (NWO).

## 415 References

- 416 1. Weinstein, I. B. Addiction to Oncogenes—the Achilles Heel of Cancer. *Science* **297**, 63–64 (July 417 2002).
- 418 2. Holohan, C., Van Schaeybroeck, S., Longley, D. B. & Johnston, P. G. Cancer Drug Resistance: An 419 Evolving Paradigm. *Nature Reviews Cancer* **13**, 714–726 (Oct. 2013).
- 420 3. Konieczkowski, D. J., Johannessen, C. M. & Garraway, L. A. A Convergence-Based Framework for 421 Cancer Drug Resistance. *Cancer Cell* **33**, 801–815 (May 2018).
- 422 4. Flaherty, K. T. *et al.* Improved Survival with MEK Inhibition in BRAF-Mutated Melanoma. *New 423 England Journal of Medicine* **367**, 107–114 (July 2012).
- 424 5. Long, G. V. *et al.* Combined BRAF and MEK Inhibition versus BRAF Inhibition Alone in Melanoma. 425 *New England Journal of Medicine* **371**, 1877–1888 (Nov. 2014).
- 426 6. Boshuizen, J. & Peepoer, D. S. Rational Cancer Treatment Combinations: An Urgent Clinical Need. 427 *Molecular Cell* **78**, 1002–1018 (June 2020).
- 428 7. Fernandes Neto, J. M. *et al.* Multiple Low Dose Therapy as an Effective Strategy to Treat EGFR 429 Inhibitor-Resistant NSCLC Tumours. *Nature Communications* **11**, 3157 (June 2020).
- 430 8. Ryan, M. B. *et al.* Vertical Pathway Inhibition Overcomes Adaptive Feedback Resistance to 431 KRASG12C Inhibition. *Clinical Cancer Research*, clincanres.3523.2019 (Nov. 2019).
- 432 9. Ozkan-Dagliyan, I. *et al.* Low-Dose Vertical Inhibition of the RAF-MEK-ERK Cascade Causes 433 Apoptotic Death of KRAS Mutant Cancers. *Cell Reports* **31**, 107764 (June 2020).
- 434 10. Zoetemelk, M. *et al.* Optimized Low-Dose Combinatorial Drug Treatment Boosts Selectivity and 435 Efficacy of Colorectal Carcinoma Treatment. *Molecular Oncology* **n/a** (2020).
- 436 11. Caumanns, J. J. *et al.* Low-Dose Triple Drug Combination Targeting the PI3K/AKT/mTOR Pathway 437 and the MAPK Pathway Is an Effective Approach in Ovarian Clear Cell Carcinoma. *Cancer Letters* 438 **461**, 102–111 (Oct. 2019).
- 439 12. Van Cutsem, E. *et al.* BEACON CRC Study Safety Lead-in (SLI) in Patients with BRAFV600E 440 Metastatic Colorectal Cancer (mCRC): Efficacy and Tumor Markers. *Journal of Clinical Oncology* 441 **36**, 627–627 (Feb. 2018).
- 442 13. Van Cutsem, E. *et al.* Binimetinib, Encorafenib, and Cetuximab Triplet Therapy for Patients With 443 BRAF V600E–Mutant Metastatic Colorectal Cancer: Safety Lead-In Results From the Phase III 444 BEACON Colorectal Cancer Study. *Journal of Clinical Oncology* **37**, 1460–1469 (June 2019).
- 445 14. Zhong, L. *et al.* Small molecules in targeted cancer therapy: advances, challenges, and future 446 perspectives. *Signal Transduct Target Ther* **6**, 201 (May 2021).
- 447 15. Nowak-sliwinska, P. *et al.* Optimization of Drug Combinations Using Feedback System Control. 448 *Nature Protocols* **11**, 302–315 (2016).
- 449 16. Weiss, A. *et al.* A Streamlined Search Technology for Identification of Synergistic Drug Combinations. 450 *Scientific reports* **5**, 14508 (2015).

451 17. Bosdriesz, E. *et al.* Comparative Network Reconstruction Using Mixed Integer Programming.  
452 *Bioinformatics* **34**, i997–i1004 (Sept. 2018).

453 18. Dorel, M. *et al.* Modelling Signalling Networks from Perturbation Data. *Bioinformatics* (2018).

454 19. Klinger, B. *et al.* Network Quantification of EGFR Signaling Unveils Potential for Targeted Combination  
455 Therapy. *Molecular systems biology* **9** (Jan. 2013).

456 20. Halasz, M., Kholodenko, B. N., Kolch, W. & Santra, T. Integrating Network Reconstruction with  
457 Mechanistic Modelling to Predict Cancer Therapy. *Science signaling* **9**, ra114 (2016).

458 21. Saez-Rodriguez, J. *et al.* Discrete Logic Modelling as a Means to Link Protein Signalling Networks  
459 with Functional Analysis of Mammalian Signal Transduction. *Molecular systems biology* **5**, 331 (Jan.  
460 2009).

461 22. Jastrzebski, K. *et al.* Integrative Modeling Identifies Key Determinants of Inhibitor Sensitivity in  
462 Breast Cancer Cell Lines. *Cancer Research* **78**, 4396–4410 (Aug. 2018).

463 23. Kirouac, D. C. *et al.* Computational Modeling of ERBB2-Amplified Breast Cancer Identifies Combined  
464 ErbB2/3 Blockade as Superior to the Combination of MEK and AKT Inhibitors. *Science signaling* **6**,  
465 ra68 (Aug. 2013).

466 24. Nyman, E. *et al.* Perturbation Biology Links Temporal Protein Changes to Drug Responses in a  
467 Melanoma Cell Line. *PLOS Computational Biology* **16**, e1007909 (July 2020).

468 25. Saez-Rodriguez, J. *et al.* Comparing Signaling Networks between Normal and Transformed Hepa-  
469 tocytes Using Discrete Logical Models. *Cancer research* **71**, 5400–5411 (Aug. 2011).

470 26. Korkut, A. *et al.* Perturbation Biology Nominates Upstream–Downstream Drug Combinations in  
471 RAF Inhibitor Resistant Melanoma Cells. *eLife* **4**, 1–31 (2015).

472 27. Soule, H. D. *et al.* Isolation and Characterization of a Spontaneously Immortalized Human Breast  
473 Epithelial Cell Line, MCF-10. *Cancer Research* **50**, 6075–86 (1990).

474 28. Di Nicolantonio, F. *et al.* Replacement of Normal with Mutant Alleles in the Genome of Normal  
475 Human Cells Unveils Mutation-Specific Drug Responses. *Proceedings of the National Academy of  
476 Sciences of the United States of America* **105**, 20864–20869 (Dec. 2008).

477 29. Korkola, J. E. *et al.* Decoupling of the PI3K Pathway via Mutation Necessitates Combinatorial  
478 Treatment in HER2+ Breast Cancer. *PLOS ONE* **10**, e0133219 (July 2015).

479 30. Gustin, J. P. *et al.* Knockin of Mutant PIK3CA Activates Multiple Oncogenic Pathways. *Proceedings  
480 of the National Academy of Sciences of the United States of America* **106**, 2835–2840 (Feb. 2009).

481 31. Haagensen, E. J. *et al.* Pre-Clinical Use of Isogenic Cell Lines and Tumours in Vitro and in Vivo for  
482 Predictive Biomarker Discovery; Impact of KRAS and PI3KCA Mutation Status on MEK Inhibitor  
483 Activity Is Model Dependent. *European Journal of Cancer* **56**, 69–76 (Mar. 2016).

484 32. Torrance, C. J., Agrawal, V., Vogelstein, B. & Kinzler, K. W. Use of Isogenic Human Cancer Cells for  
485 High-Throughput Screening and Drug Discovery. *Nature Biotechnology* **19**, 940–945 (Oct. 2001).

486 33. Martin, T. D. *et al.* A Role for Mitochondrial Translation in Promotion of Viability in K-Ras Mutant  
487 Cells. *Cell Reports* **20**, 427–438 (July 2017).

488 34. De Lint, K. *et al.* Sensitizing Triple-Negative Breast Cancer to PI3K Inhibition by Cotargeting IGF1R.  
489 *Molecular Cancer Therapeutics* **15**, 1545–1556 (July 2016).

490 35. Iorio, F. *et al.* A Landscape of Pharmacogenomic Interactions in Cancer. *Cell* **166**, 740–754 (2016).

491 36. Vis, D. J. *et al.* Multilevel Models Improve Precision and Speed of IC<sub>50</sub> Estimates. *Pharmacoge-  
492 nomics* **17**, 691–700 (May 2016).

493 37. Kholodenko, B. N. *et al.* Untangling the Wires: A Strategy to Trace Functional Interactions in  
494 Signaling and Gene Networks. *Proceedings of the National Academy of Sciences of the United  
495 States of America* **99**, 12841–6 (Oct. 2002).

496 38. R Core Team. *R: A Language and Environment for Statistical Computing* R Foundation for Statistical  
497 Computing (Vienna, Austria, 2021).

498 39. Kuhn, M. & Wickham, H. *Tidymodels: a collection of packages for modeling and machine learning  
499 using tidyverse principles.* (2020).

500 40. Virtanen, P. *et al.* SciPy 1.0: Fundamental Algorithms for Scientific Computing in Python. *Nature  
501 Methods* **17**, 261–272 (2020).

502 41. Wolfram Research, Inc. *Mathematica, Version 12.0* Champaign, IL, 2019.

503 42. Wei, T. & Simko, V. *R package 'corrplot': Visualization of a Correlation Matrix* (Version 0.92) (2021).

504 **Supplementary Figures**

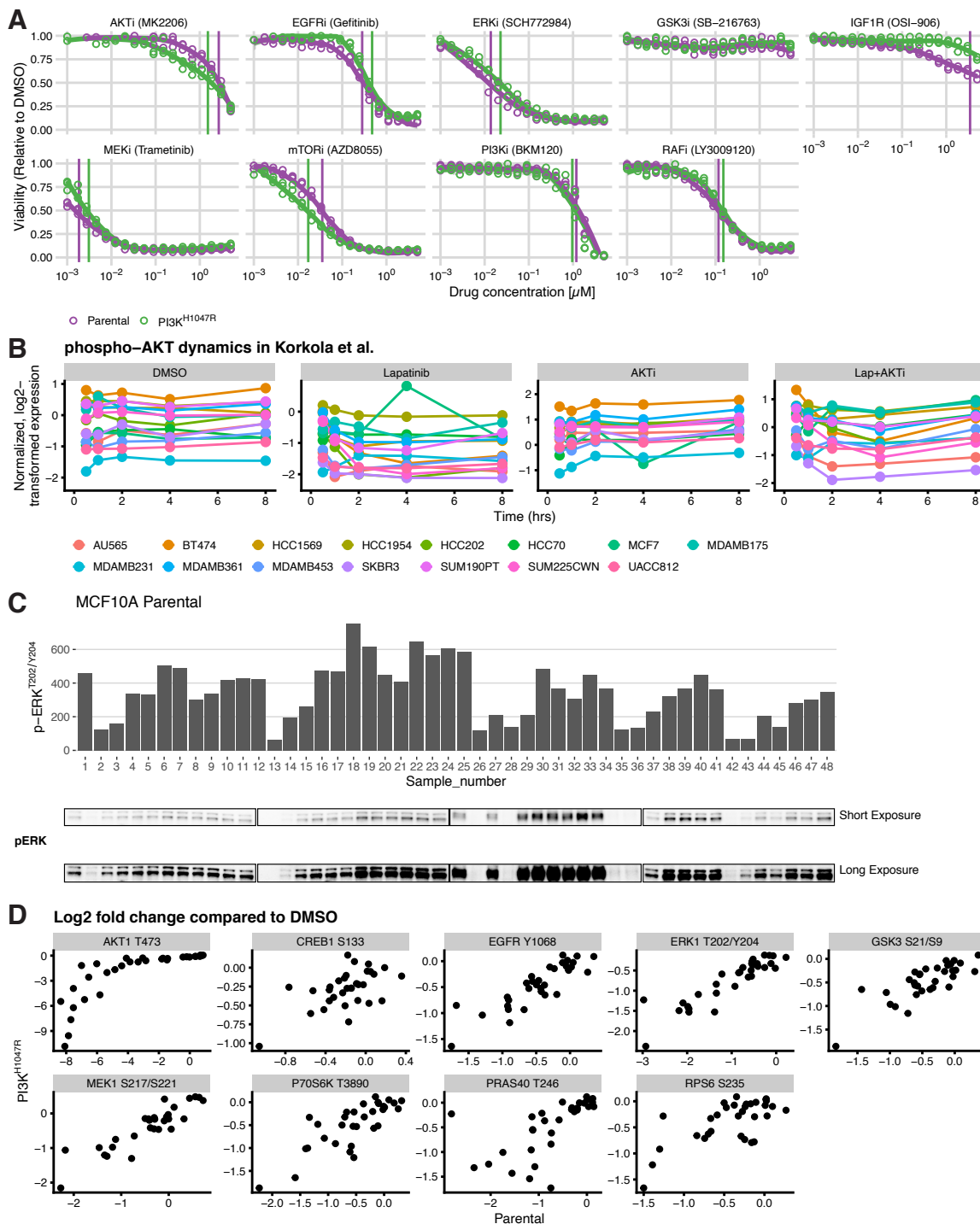


**Figure S1: A.** Dose-response curves of the inhibitors used in this study. **B.** Dynamics of AKT activity after PI3K pathway inhibition from Korkola *et al.* [29] **C.** Correlation between phospho-ERK quantification using Luminex (top) and Western blot (bottom). **D.** Correlation between the response in parental (x-axis) and  $\text{PI3K}^{\text{H}1047\text{R}}$  (y-axis) cells. Response is defined as  $\log_2$ -fold change compared to DMSO controls.

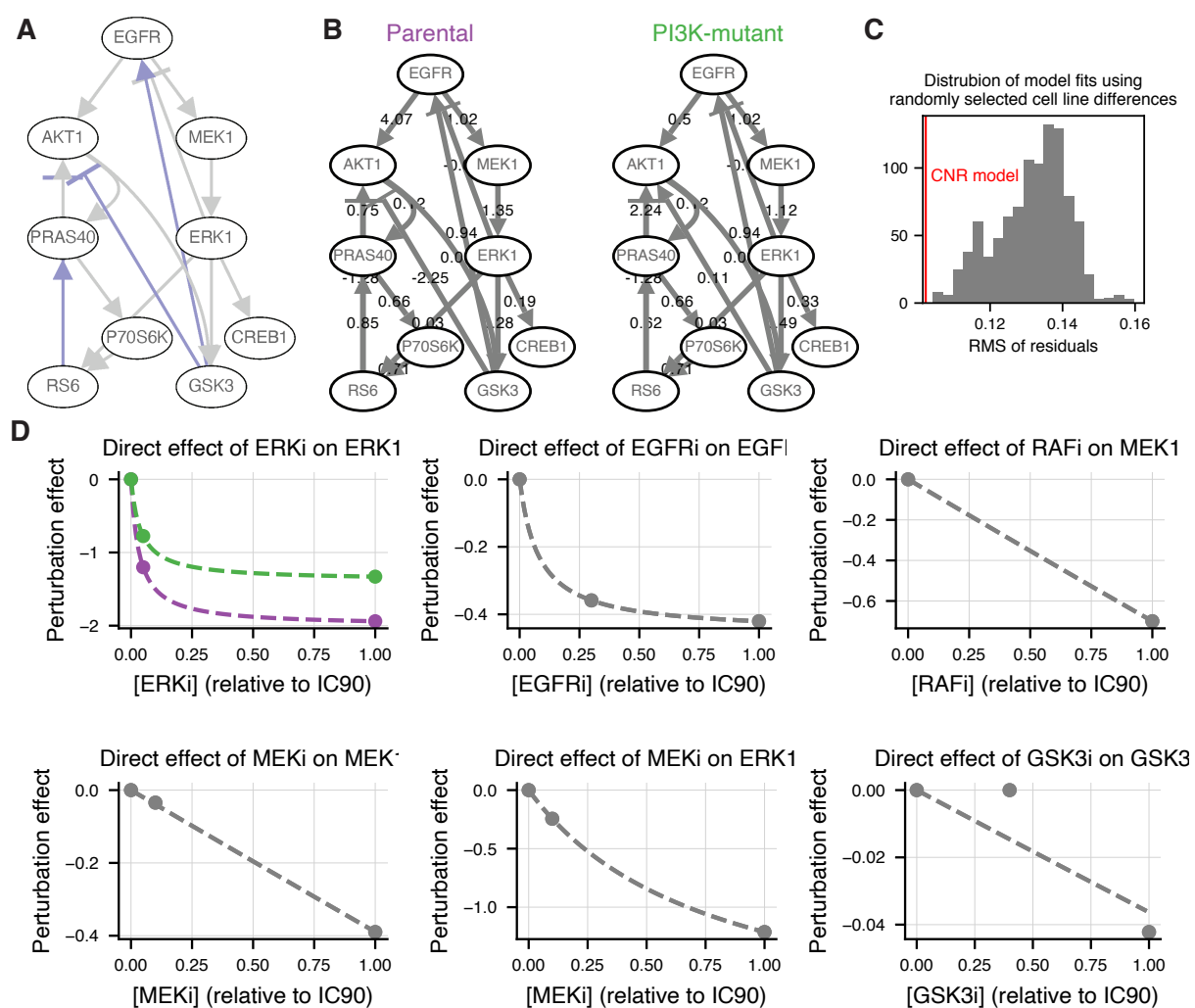


**Figure S2: A.** Network topology used for modeling. Edges used as prior information are indicated in gray. Edges added in a leave one out cross validation loop are indicated in purple. **B.** Network models of the parental (left) and PI3K<sup>H1047R</sup> cells. Edge labels indicate reconstructed interaction strengths ( $r_{ij}$  terms in Equation 2 and 3). **C.** Significance of identified differences between the cell lines. Distribution of the residuals of 1000 model optimizations in which random edges were selected to allow to differ between the two cell. The selected model has a better model fit than all 1000 of these models. **D.** The estimated direct effect of different inhibitors on their target, as a function of applied inhibitor concentration ( $s_{ij}$  terms in Equation 2 and 3). Points indicate the estimated effects obtained from the CNR reconstruction, at the concentrations used in the perturbation experiments. The dashed lines indicate the interpolated curves between these points. (c.f. Materials and Methods, Equation 5)

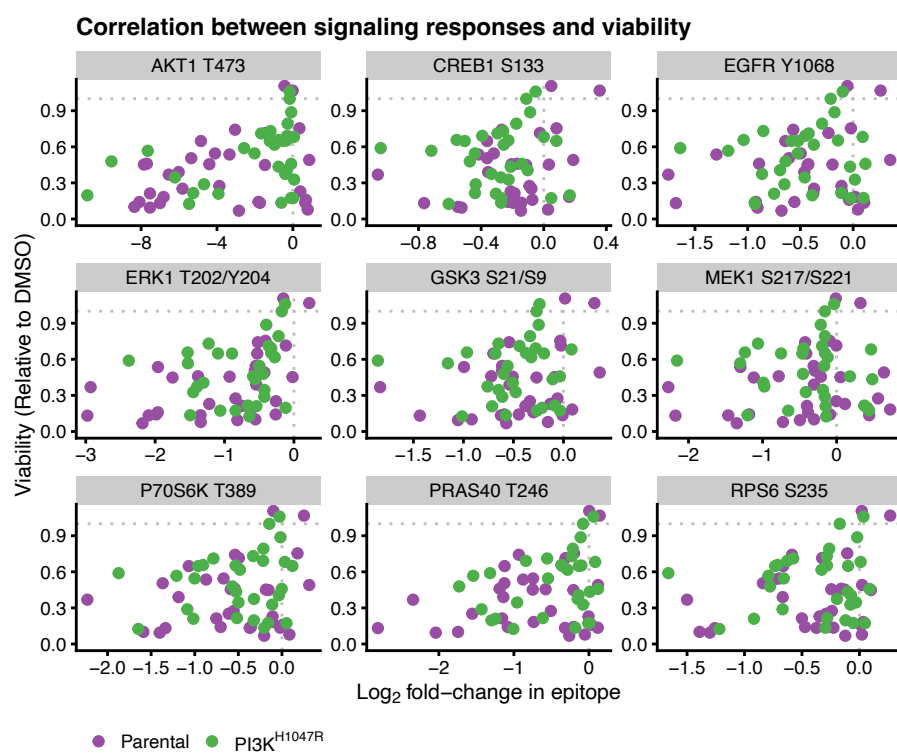


**Figure S3:** Correlation between node response and cell viability of all measured nodes.

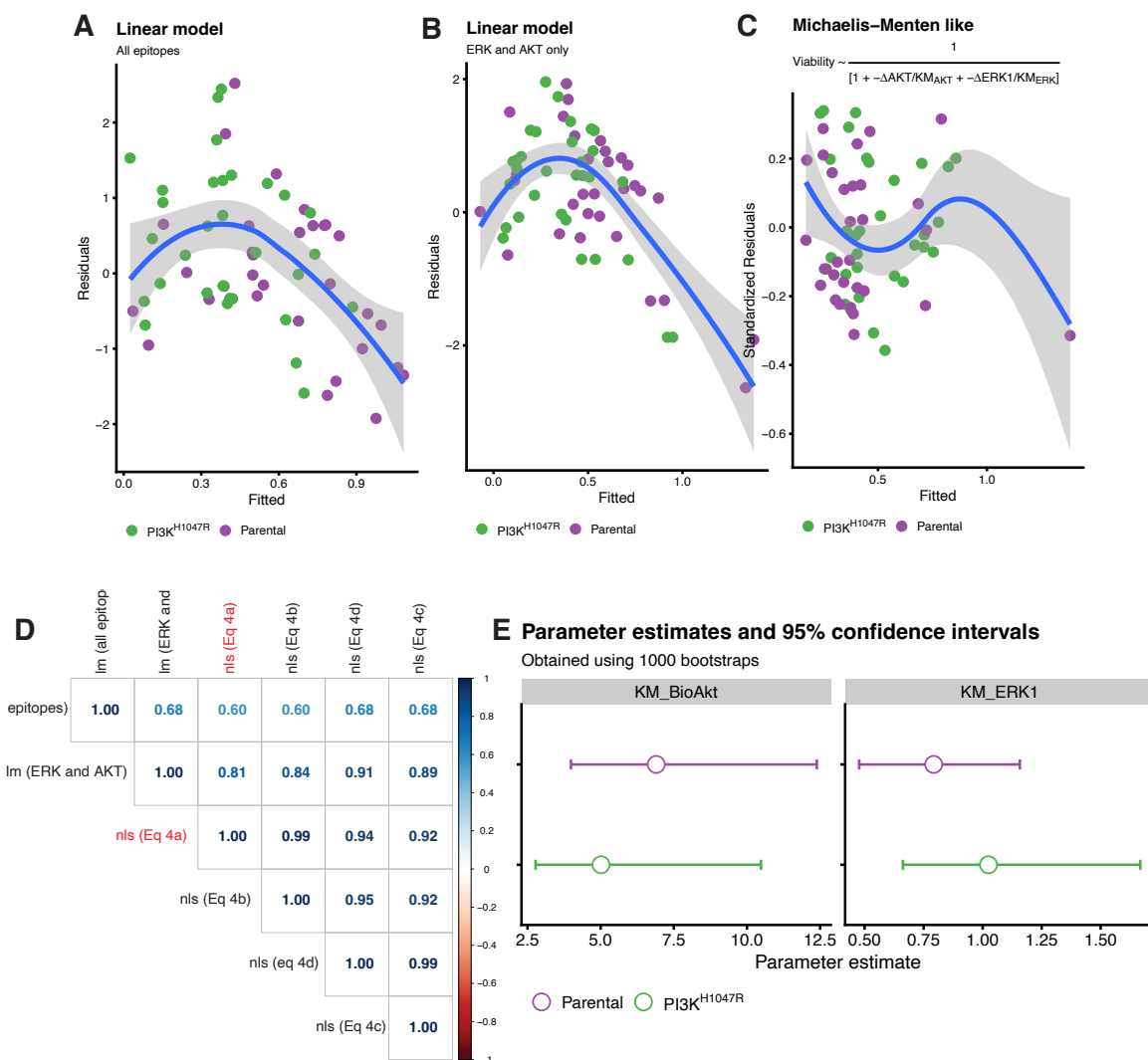


**Figure S4: Evaluation of model fits relating signaling response to cell viability.** **A-C.** Residuals as a function of fitted values for the model fits. **A.** Linear model with all epitopes as predictor. **B.** Linear model with only  $R_{AKT}$  and  $R_{ERK}$  as predictor. **C.** Non-linear model that gave the best fit ( Equation 4c). **D.** Pearson correlation between model predictions of all models tested show that the predictions of all non-linear models are highly similar. Predictions are obtained from the leave-one-out cross-validation. The selected model (Equation 4c) is highlighted in red. The plot is generated using the `corrplot`-function of the `corrplot` R-package [42]. **E.** Bootstrapping intervals of the estimated values for the parameters  $K_{M,AKT}$  and  $K_{M,ERK}$  in Equation 4c

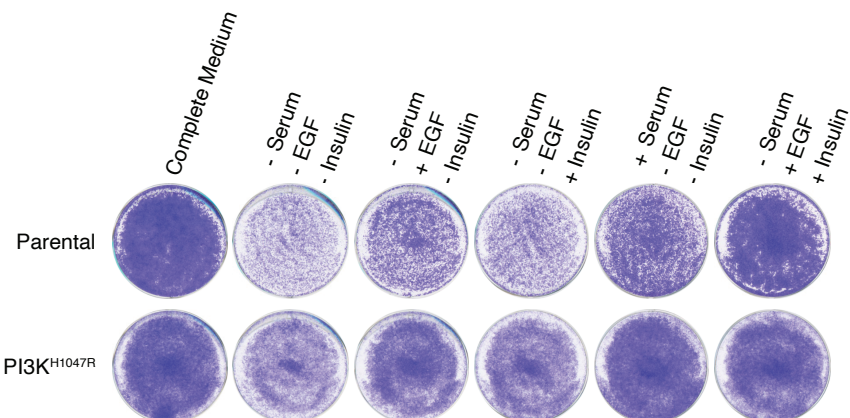


**Figure S5:** Growth of MCF10A parental and PI3K<sup>H1047R</sup> cells in different growth media. In contrast to the parental cells the PI3K mutant cells grow well in the absence of serum if either Insulin or EGF is provided.

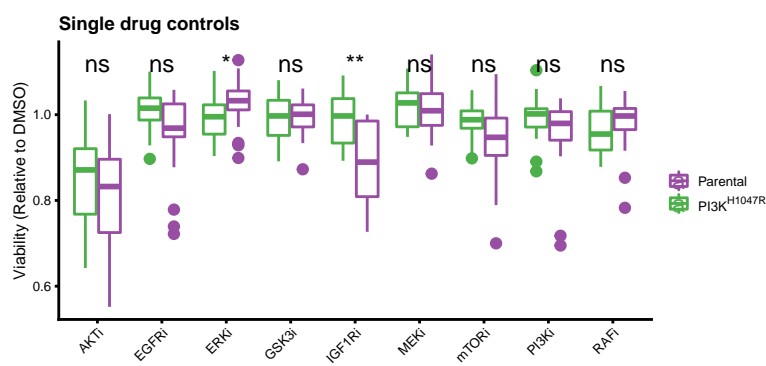


**Figure S6:** Viability of the low-dose single-drug controls, all measured at their  $IC_{10}$ . Except for IGF1Ri, none of the drugs show selectivity towards the parental cells. Treatments were performed in 8 replicates.